How to cite: *Angew. Chem. Int. Ed.* **2024**, *63*, e202406385
doi.org/10.1002/anie.202406385

Photocatalysis **Hot Paper**

Photochargeable Mn-Based Metal–Organic Framework and Decoupled Photocatalysis

*Shufan Wu, Philip M. Stanley, Simon N. Deger, Mian Zahid Hussain, Andreas Jentys, and Julien Warnan**

Abstract: Designing multifunctional materials that mimic the light-dark decoupling of natural photosynthesis is a key challenge in the field of energy conversion. Herein, we introduce **MnBr-253**, a precious metal-free metal–organic framework (MOF) built on Al nodes, bipyridine linkers and $MnBr(CO)_3$(bipyridine) complexes. Upon irradiation, **MnBr-253** colloids demonstrate an electron photocharging capacity of ~42 $C \cdot g^{-1}_{MOF}$, with state-of-the-art photocharging rate (1.28 $C \cdot s^{-1} \cdot g^{-1}_{MOF}$) and incident photon-to-electron conversion efficiency of ~9.4 % at 450 nm. Spectroscopic and computational studies support effective electron accumulation at the Mn complex while high porosity and Mn loading account for the notable electron storage performance. The charged **MnBr-253** powders were successfully applied for hydrogen evolution under dark conditions thus emulating the light-decoupled reactivity of photosynthesis.

As global energy demand rises, efficient energy collection, storage, and utilization of have become critical for the development of human society.[1] Sunlight, as an inexhaustible clean energy source, remains a central focus in energy research, and particularly its efficient conversion into directly usable and storable energies.[2] Natural evolution has answered the solar energy storage challenge with photosynthesis, allowing plants, algae, and cyanobacteria, to convert absorbed solar energy into chemicals independently of light. Such flexibility in artificial electro-systems could enable decoupled solar harvesting and fuel production or long-term electron storage, avoiding multiple electro-synthetic steps, chemical fuel storage, while offering flexibility in energy carrier form and temporal demand.[3] In this context, the advancement of materials, capable of both solar energy harvesting, and electron storage is key albeit at a nascent stage.[4] Polyoxometalate, carbon nitride, metal oxide materials have already demonstrated potentials toward charged off-grid, wireless colloidal systems but continued efforts to broaden the material scope and enhanced overall performance are critical.[5]

Metal–organic frameworks (MOFs), composed of organic ligands and metal nodes, offer ideal platforms for developing energy applications due to their crystallinity, porosity, and customizable three-dimensional structures.[6] Toward light-induced electron storage, promising examples include linker-engineered Ti-based MIL-125 and MOF-253 modified with Lehn-type Re complexes, showing light absorption, sacrificial electron donor (SED) oxidation and electron accumulation within the framework for later use in dark photocatalysis.[7] Despite these recent advances, modest accessibility to the electroactive sites, low visible light absorption, poor stability underscore the need for further efforts.

Herein, we introduce **MnBr-253** as a photochargeable rare metal-free hybrid material, made of Al nodes, bipyridine linkers and *fac*-[$MnBr(CO)_3$(dcbpy)] (dcbpy = 5,5'-dicarboxylic-2,2′-bipyridine) complexes (Figure 1). Mn 2,2′-bipyridyl (bpy) tricarbonyl halide (X) complexes constitute a versatile family of photoredox structure, however, impeded by photodegration.[8] Building on our prior work on Re MOF-253′s electron accumulation, we explored Mn-functionalized MOF-253′s photocharging ability and photostability.[7b] As Earth crust's third most abundant transition metal, Mn is a promising alternative to Re, with their complexes likely sharing similar opto-electronic properties and reactivities as extensively shown for CO_2 reduction studies.[9] Considering porous materials, Mn is lighter and smaller potentially limiting diffusion-related issue and device integration hinderance.[10]

MnBr-253 enables visible light energy harvesting and electron storage from electron source photo-oxidation, reaching up to ~42 $C g^{-1}_{MOF}$ and a state-of-the-art incident photon-to-electron conversion/storage quantum yield (AQY) of ~9.4 % at 450 nm. The electron storage ability was employed to drive catalytic H_2 evolution reaction

[*] S. Wu, Dr. P. M. Stanley, S. N. Deger, Dr. M. Z. Hussain, Dr. J. Warnan
Chair of Inorganic and Metal-Organic Chemistry
Department of Chemistry, and Catalysis Research Center (CRC)
TUM School of Natural Sciences
Technical University of Munich
Garching, Germany
E-mail: julien.warnan@tum.de

Prof. Dr. A. Jentys
Chair of Industrial Chemistry and Heterogenous Catalysis
Department of Chemistry, and Catalysis Research Center (CRC)
TUM School of Natural Sciences
Technical University of Munich
Garching, Germany

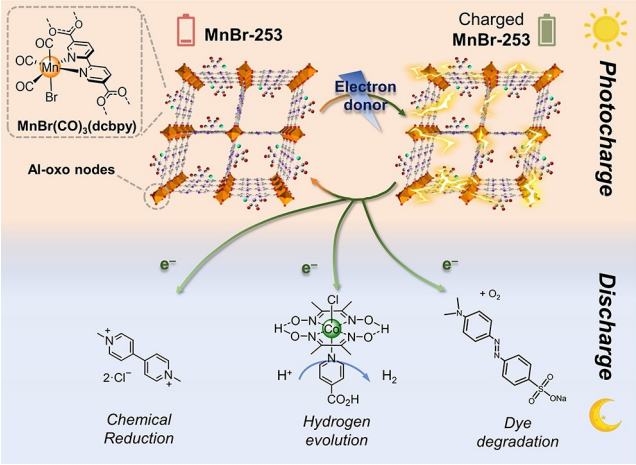

Figure 1. Schematic representation of **MnBr-253**'s structure, composition, working principle, and dark applications (including, from left to right, methyl viologen dichloride, $Co(dmgH)_2$(4-pyridinecarboxylic acid) (dmgH = dimethylglyoxime) and methyl orange structures).

(HER) and O_2-assisted dye degradation under lightless conditions, demonstrating temporal decoupling of energy harvesting and utilization. Density functional theory (DFT)-based calculations, electron paramagnetic resonance (EPR) characterizations together elucidate that the hour-lived electrons are confined as bipyridyl radical anions at the Mn-bpy centers.

MOF-253 was synthesized from 5,5'-dicarboxylic-2,2′-bipyridine and $AlCl_3$ following a modified reported procedure (details in Supporting Information, SI, Figure S1) involving sonication and MOF activation at 150 °C for 18 hours.[7b] The white MOF-253 powder was dispersed in a $MnBr(CO)_5$ acetonitrile solution and heated to 50 °C for 24 hours to produce *fac*-[$MnBr(CO)_3$(5,5'-dcbpy)] moieties. **MnBr-253** was isolated as a brick-red powder and characterized (Figure 2). Its powder X-Ray diffraction (PXRD) pattern matched MOF-253′s, suggesting maintained overall crystallinity post-Mn integration (Figure 2a). In contrast to that of MOF-253, the attenuated total reflectance infrared (ATR-IR) spectrum of **MnBr-253** displayed bands at 2031.7 and 1944.8 cm^{-1} ascribed to the carbonyl asymmetric stretching vibrations, ν(C≡O) (Figure 2b).[11] These bands differ from that of the $MnBr(CO)_5$ precursor suggesting selective formation of *fac*-$MnBr(CO)_3$(dcbpy) units. While the broad signal around 1944.8 cm^{-1} typically appears as two bands in discrete molecules, merging is commonly observed in immobilized systems.[12] Solid-state UV/Vis spectroscopy analysis of MOF-253 revealed no absorption beyond 350 nm. In contrast, **MnBr-253** absorbs broadly with a visible-light-centered maximum intensity absorption at 460 nm (Figure 2c) previously ascribed to metal-to-ligand charge transfer transition from the Mn to the bipyridine ligand.[12b,13]

The electronic and coordination properties of Mn in **MnBr-253** were elucidated via X-ray absorption spectroscopy. The Mn K-edge at ~6550 eV indicates an oxidation

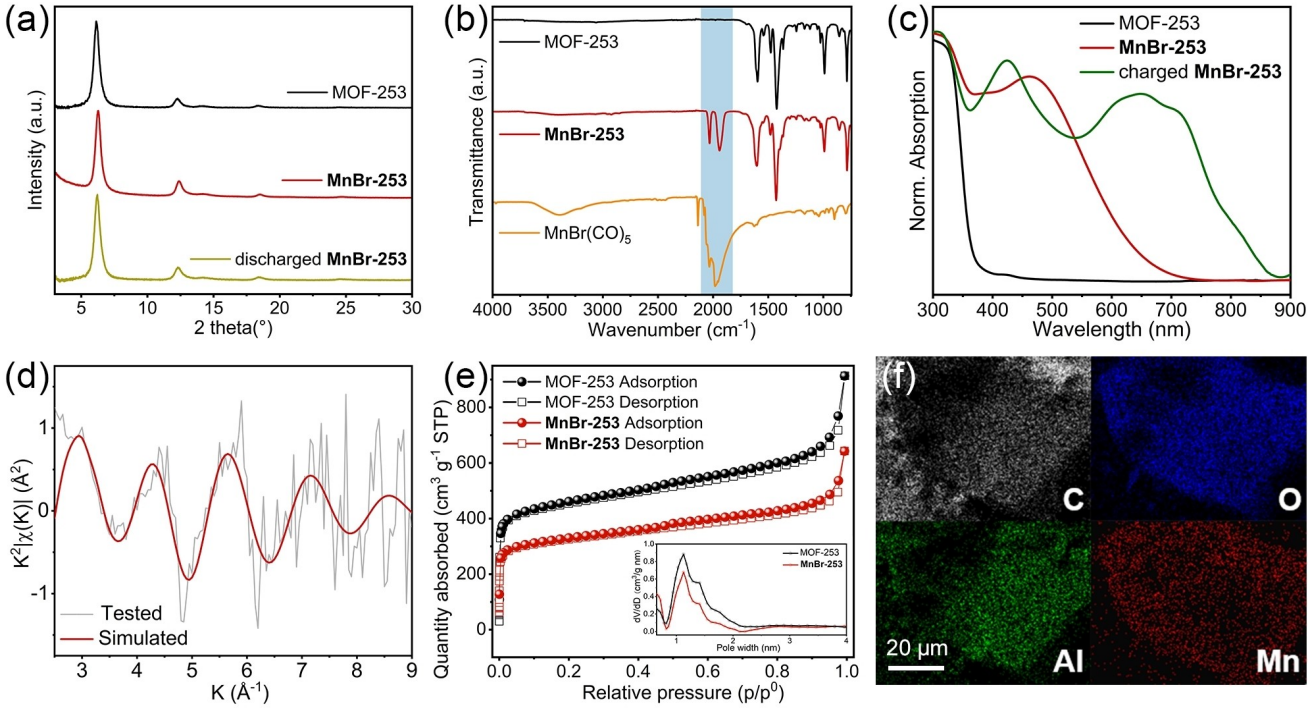

Figure 2. (a) Powder XRD patterns of MOF-253, uncharged and discharged **MnBr-253**. (b) ATR-IR spectra of MOF-253, **MnBr-253** and $MnBr(CO)_5$. (c) The solid-state UV/Vis spectra of MOF-253, uncharged and discharged **MnBr-253**. (d) Extended X-ray absorption fine structure of Mn in **MnBr-253** and results of the fit (k^2 weighted). (e) N_2 adsorption-desorption isotherms of MOF-253 and **MnBr-253** at 77 K. Inset: pore size distribution of MOF-253 and **MnBr-253**. (f) EDX mapping of **MnBr-253**.

state near 2.4 which contrast with the expected Mn(I) state. This is ascribed to X-ray-induced damage and Mn's propensity for higher oxidation states (Figure S2). Nevertheless, extended X-ray absorption fine structure (EXAFS) analysis revealed a high congruence with molecular modeling of Mn′s coordination environment (Figure 2d, Table S1) confirming a one bromine, three carbon, and two nitrogen atoms first coordination shell.

Nitrogen adsorption measurements unveiled a Brunauer–Emmett–Teller (BET) surface area of ~1657.4 and ~1228.3 $m^2 \cdot g^{-1}$ for MOF-253 and **MnBr-253** (Figure 2e, Table S2), respectively. This value is in the higher end of the surface area range and is potentially attributed to the high activation temperature used.[14] Both samples have nanopores primarily around 1 nm, with a 25.9 % decrease of total pore volume upon Mn integration ascribed to the complex's hinderance effect. Nevertheless, the material remains highly porous as a prerequisite for solution infiltration.[10,15] Scanning electron microscope analysis and energy dispersive X-ray (EDX) mapping (Figures 2f and S3–4) showed heterogeneous micromorphology at the micron level without uniform particle size and a homogeneous aggregate-free distribution of each element.

Inductively coupled plasma mass spectrometry (ICP-MS) measurements carried out on the digested **MnBr-253** revealed a relatively high Mn content of ~1 $mmol \cdot g^{-1}_{MOF}$ (inferring that on average 1 in every 3.7 bipyridines is coordinated) potentially due to the powders' high surface area (Table S3).[7b,16] Thermogravimetric analysis under Ar atmosphere revealed that MOF-253 begins to degrade at ~420 °C, while **MnBr-253** shows a preliminary mass loss of ~8.4 wt % between 160–200 °C, attributed to the release of the complex's CO ligands (Figure S5). This value broadly agrees with ICP-MS Mn loading results as the CO ligands should account for ~6.6 wt % of **MnBr-253**'s total molecular weight (calculation in SI).

Next, we studied the photo-reactivity of **MnBr-253** (Figure 3). The powder was dispersed in acetonitrile with triethanolamine (TEOA), used as SED, under Ar atmosphere. Subjected to LED irradiation for 80 min ($\lambda \approx 450$ nm, 2 mW/cm^2, denoted as "standard charging" conditions), **MnBr-253** underwent a noticeable color transition from brick red to dark green. In contrast, no color changes were observed without light, TEOA, or using MOF-253 instead of **MnBr-253** under otherwise unchanged conditions (Table S4). This highlights the key role of each item and indicates a photoinduced electron transfer from TEOA to the complex upon light absorption. The green color was found to be persistent post-irradiation (unless air exposed) allowing for powder isolation and investigations (Figure 3a).

Solid-state UV/Vis analysis of the green sample revealed two main absorption bands around 420 and ~700 nm contrasting with that of pristine **MnBr-253** (Figure 2c). Continuous-wave EPR analysis conducted on the charged **MnBr-253** exhibited a distinct isotropic signal with a g-value of 1.9959 (Figure 3b), highlighting its paramagnetic nature and the presence of organic radicals.[17] Considering this and MOF-253′s electrochemical inertness, it is anticipated that the radicals mainly localize on the Mn's bipyridyl ligands.

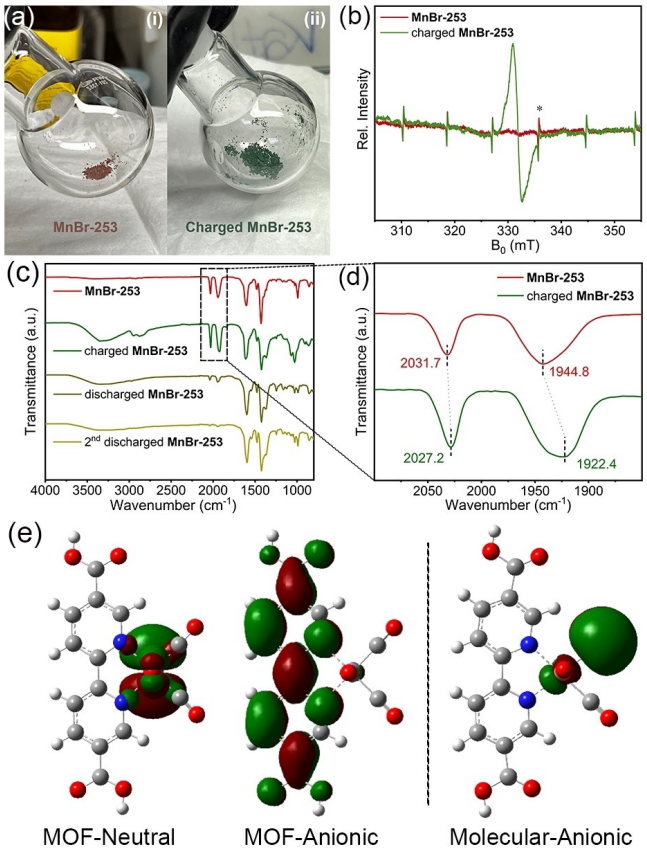

Figure 3. (a) Photograph of **MnBr-253** before (i) and after (ii) charging procedure. (b) EPR trace of **MnBr-253** and charged **MnBr-253** measured at room temperature. (c) ATR-IR spectra of uncharged, charged, discharged and 2nd discharged **MnBr-253**. (d) Partial enlargement of the ν(CO) region. (e) Electron density distribution of the HOMO or SOMO in *fac*-[$MnBr(CO)_3$(5,5′-dcbpy)] fragments depicted in their (left) neutral and (middle) radical anion states with node-coordinating oxygen atoms fixed, and as (right) a molecular radical anion complex.

Charge-compensation potentially occurs via protons released from the electron donor degradation.[18] The ATR-IR spectrum after irradiation showed no significant alteration in the organic framework vibrations ($< 1700\ cm^{-1}$) of the MOF, however, the ν(CO) bands shifted to lower frequencies (Figure 3d). This infers a higher back donation to the carbonyls, likely originating from an increased electron density (ED) near the Mn center.[19] Formation of typical photodegradation products of discrete *fac*-[$MnX(CO)_3$-(bpy)]-type complexes (e.g., *mer*-[$MnX(CO)_3$(bpy)], halide-dissociated intermediates, $Mn_2(CO)_6(bpy)_2$ dimers) was discounted as characterized by higher ν(CO) frequencies or major shifts ($> 50\ cm^{-1}$) contrasting with the modest lower-frequency changes observed here (Figure 3d).[20] While it cannot be fully excluded due to the signal's broadness, Mn coordination by TEOA is unlikely, as ν(CO) frequencies do not match prior reports and a similar trend was observed on **MnBr-253** charged with other SEDs (Figure S6).[21]

To further elucidate the color change ascription, we conducted DFT calculations. An electron was introduced on

a $[MnBr(CO)_3(dcbpy)]$ moiety in MOF-253 (using the corresponding literature-extracted single crystal linker structures) to mimic a charged state within **MnBr-253**. The node-coordinating oxygen atoms were fixed before structure optimization to further reproduce the rigid MOF structure (Figure S7, details in SI). The ED distributions for the highest and singly occupied molecular orbitals (HOMO and SOMO, respectively) were simulated for both the neutral and radical anionic states of the complex, respectively (Figure 3e). While the ED of $[MnBr(CO)_3(dcbpy)]$ mainly lies on the Mn, it shifts to the bipyridyl ligand in $[MnBr(CO)_3(dcbpy)]^{\bullet-}$. The latter's simulated ATR-IR and UV/Vis spectra exhibited behaviors consistent with experimental findings, with downward ν(CO) frequencies shifts and strong absorption around ~700 nm (Figures S8–9). Overall, DFT calculations support the formation of a radical bipyridyl anion at the Mn complex without altering the ligand shell. Interestingly, calculations performed on the radical anion $[MnBr(CO)_3(dcbpy)^{\bullet-}$ of the discrete molecule revealed a Mn-centered ED. This is coherent with the literature and the documented halide dissociation triggered by the reduction of such complexes. This highlights the major impact of MOF integration on the complex's properties, attributed to the electron-withdrawing nature of the MOF-rigidified dcbpy ligand.[7b,22] With the Mn center's lowered reactivity, stability is improved unlocking the observed electron confinement behavior.

With photocharging materials holding great promises toward dark photocatalysis, sensor or memory device, we investigated **MnBr-253**'s main redox features.[4b] Our attempt to synthesize molecular *fac*-$[MnBr(CO)_3(5,5'\text{-dcbpy})]$ revealed its fast degradation (~5 min) precluding investigation of its reduction potential (E_{red}).[11] E_{red} was broadly anticipated around −0.6 V vs normal hydrogen electrode (V_{NHE}) based on prior reports on *fac*-$[ReBr(CO)_3(5,5'\text{-dcbpy})]$ and the higher electronic affinity of Mn complexes.[23] The electron quantification in charged **MnBr-253** was achieved upon using methyl viologen dichloride (MV) as an electron accepting titrant ($E_{red}(MV) \approx -0.45$ V_{NHE}) (details available in SI).[24] In short, **MnBr-253** was irradiated under "standard charging" conditions for various times before injecting an Ar-purged MV solution in the dark. A rapid solution color change was observed from colorless to blue with concomitant disappearance of **MnBr-253**'s green color. Supernatant UV/Vis spectroscopy displayed absorption spectra consistent with that of $MV^{\bullet-}$ and showed an intensity increase over irradiation time, peaking after 80 minutes (Figure S10, Table S5). Beer–Lambert $[MV^{\bullet-}]$ analysis indicated that $14.3 \pm 1.1\ C \cdot g^{-1}_{MOF}$ was originally accumulated in **MnBr-253**.

Given the critical importance of the photocharging rate (R_{PC}) for applications, we investigated faster charging by increasing the irradiance from 2 to 10 to 20 mW/cm^2. A dramatic reduction of the maximum-charging time was achieved shifting from 80 to 20 to 1 minute, respectively (Figures S10–12, Tables S5–7). Concurrently, the maximum electron storage capacity almost doubled, reaching $27.0 \pm 1.8\ C \cdot g^{-1}_{MOF}$. Next, we investigated the impact of the SED replacing TEOA by triethylamine (TEA) (Figure 4). While both are common SEDs, TEA, with smaller monomolecular radius than TEOA (3.44 vs 4.45 Å, Figure 4a), is potentially more effective, especially in infiltrating porous materials. Under 20 mW/cm^2 irradiation with TEA (denoted as "optimized charging" conditions), a maximum charge accumulation of $41.5 \pm 3.6\ C \cdot g^{-1}_{MOF}$ ($\delta_{max} = 4.36 \times 10^{-4}\ mol_{e^-} \cdot g^{-1}_{MOF}$) was achieved within one minute, revealing the superior reactivity of TEA. After 30 seconds a charging power of $1.28\ C \cdot s^{-1} \cdot g^{-1}_{MOF}$ ($R_{PC} = 1.35 \times 10^{-5}\ mol_{e^-} \cdot g^{-1}_{MOF} \cdot s^{-1}$) was calculated, corresponding to a remarkable AQY of 9.4 % at 450 nm, underscoring **MnBr-253**'s outstanding capability for rapid and efficient charge accumulation (Figure S13, Table S8).[4a]

Prolonged irradiation led to electron loss, which occurred at slower rates with decreasing irradiance signaling its influence on both charging and degradation processes (Figure 4a). Over time in the dark, the material exhibited hour-long charge storage but experienced gradual decay, with approximately 50 % of the initial charge lost after 3 hours at 4 °C (Figure S14, Table S9). After a photocharging/discharging process under standard conditions, a

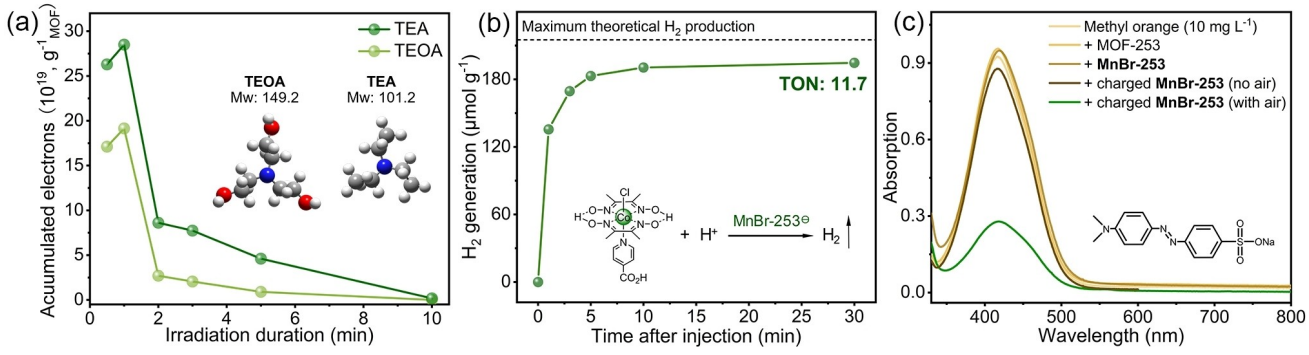

Figure 4. (a) Accumulated electron in **MnBr-253** after different irradiation time when using TEOA or TEA as the electron source. Inset displays the molecular model and weight of TEOA and TEA. (grey: carbon, blue: nitrogen, red: oxygen, white: hydrogen) (b) H_2 evolution vs time upon the injection of a Co catalyst solution to a charged **MnBr-253** (**MnBr-253**$^{\ominus}$) solution in the dark. (c) UV/Vis spectra of a methyl orange solution (10 mg L^{-1}) before and after being exposed to MOF-253, **MnBr-253**, charged **MnBr-253** (injected as an Ar-purged solution, no air) or charged **MnBr-253** (injected as-prepared, with air).

second cycle demonstrated some rechargeability of the MOF, but reached only ~10 % of the original value (Figure S15, Table S10). ATR-IR, solid-state UV/Vis and PXRD analysis of the discharged **MnBr-253** samples revealed low ν(CO) band intensities, modest absorption band at ~450 nm and new reflections, respectively (Figures 3c, S16–17), indicating that both the Mn complex and the MOF structure are affected by the photocycles. EXAFS analysis further confirmed the complex's partial structural decomposition and formation of Mn–O bonds possibly at the node units (Figure S18, Table S11). The low stability of the reduced Mn complex might be ascribed to the slow dissociation of the Br ligand and subsequent complex degradation.[25] The observed photodegradations align with the light-sensibility of $[MnX(CO)_3(bpy)]$ complexes and are potentially accelerated by the strong absorption abilities of $[MnBr(CO)_3(dcbpy)]^{\bullet-}$, generating highly reactive excited species (Figure 2c).[13,26] Nonetheless, considering that the discrete $[MnBr(CO)_3(dcbpy)]$ complex degrades within minutes, halide dissociation typically occurs upon reduction, and $[MnX(CO)_3(bpy)]$ complexes are light-unstable, integration within the MOF delivered remarkable stability improvement and incidentally highlights the benefits of interfacing complexes with MOFs.

The high charge capacity, rapid photo-charging and discharging and reductive potential of **MnBr-253** creates opportunity toward delayed "dark" photochemistry. HER catalysis and organic dye degradation were investigated as model reactions for energy conversion and environmental remediations. For HER catalysis, a benchmark cobaloxime catalyst (Figure 1), was dissolved in an Ar-purged H_2O/MeCN (10/1, v/v) solvent mixture and injected into the charged **MnBr-253** system in the dark.[27] The green color of **MnBr-253** faded immediately, and gas chromatography headspace analysis revealed rapid catalytic H_2 production (Figure 4b and Table S12), with 70 % of the charges accounted for after 1 min, representing a conservative rate of discharging (R_{DC}) of $4.53\times10^{-6}\,mol_{e-}\cdot g^{-1}{}_{MOF}\cdot s^{-1}$. Total turnover number (TON) per Co levelled around 11.5 after 10 minutes accounting for a 90 % electron conversion efficiency. The unaccounted 10 % are potentially due to the Co(III)-to-Co(II) reduction required before the catalytic cycle occurs and to Mn complex degradation. Alternatively to adding the Co catalyst, methyl orange (MO) was employed, as a representative waterborne dye pollutant.[28] Injecting a non-degassed MO solution into a charged **MnBr-253** solution promptly reduced MO absorption at ~420 nm (Figure 4c). Control experiments performed without the main reactants (e.g., O_2 or Co catalyst) or light confirmed the electron cascade from **MnBr-253** to H_2 or degraded MO, mediated by the catalyst or O_2, respectively (Tables S13–15).

In summary, the development of **MnBr-253** particles represents a significant advance in circuitry-free energy materials, mimicking the light-dark decoupled reactivity of photosynthesis. Computational and experimental approaches elucidated the mechanism of charge storage as bipyridyl radical anions. The system achieves benchmarking AQY of ~9 % while delivering state-of-the-art charge accumulation after 1 min of visible light irradiation. Swift charge in-take and on demand release open avenues for off-grid applications, exemplified here with catalytic H_2 evolution, as well as potential for implementation in photoelectrochemical devices (e.g., battery and capacitor).[29] Despite stability issues, **MnBr-253** demonstrates remarkable resilience and reactivity compared to its molecular counterparts suggesting opportunities to stabilize reactive coordination complexes in MOFs.

Acknowledgements

This work was supported by the German Research Foundation (DFG) and the Excellence Cluster 2089 "e-conversion" (Fundamentals of Energy Conversion Processes). The easyXAFS300+ system was supported by the DFG (Project 451579122). Shufan Wu thanks the financial support from the China Scholarship Council (CSC). The authors are grateful for the helpful discussions and the support from Roland A. Fischer. The authors thank Katia Rodewald for SEM images and EDX measurements as well as Oksana Storcheva for the EPR measurements. Open Access funding enabled and organized by Projekt DEAL.

Conflict of Interest

The authors declare no conflict of interest.

Data Availability Statement

The data that support the findings of this study are available from the corresponding author upon reasonable request.

Keywords: Metal–Organic Framework · Mn complex · Electron accumulation · Photocharging · Dark Photocatalysis

[1] United Nations Treaty Collection, *Paris Agreement*, Paris, **2015**.
[2] a) N. S. Lewis, *Science* **2016**, *351*, aad1920; b) D. G. Nocera, *Acc. Chem. Res.* **2017**, *50*, 616; c) A. A. İnada, S. Arman, B. Safaei, *J. Energy Storage* **2022**, *55*, 105661; d) J. Lv, J. Xie, A. G. A. Mohamed, X. Zhang, Y. Feng, L. Jiao, E. Zhou, D. Yuan, Y. Wang, *Nat. Chem. Rev.* **2023**, *7*, 91.
[3] a) B. Rausch, M. D. Symes, G. Chisholm, L. Cron, *Science* **2014**, *345*, 1326; b) D. Schmidt, M. D. Hager, U. S. Schubert, *Adv. Energy Mater.* **2015**, *6*, 1500369; c) Q. Zeng, Y. Lai, L. Jiang, F. Liu, X. Hao, L. Wang, M. A. Green, *Adv. Energy Mater.* **2020**, *10*, 1903930; d) L. Zhang, Y. Wang, *Angew. Chem. Int. Ed. Engl.* **2023**, *62*, e202219076.
[4] a) O. Savateev, *Adv. Energy Mater.* **2022**, *12*, 2200352; b) A. Rogolino, O. Savateev, *Adv. Funct. Mater.* **2023**, *33*, 2305028.
[5] a) M. G. Russell, F. Howe, *J. Phys. Chem.* **1985**, *89*, 4495; b) A. Henglein, *Ber. Bunsen. Phys. Chem.* **2010**, *86*, 241; c) V. W. Lau, D. Klose, H. Kasap, F. Podjaski, M. C. Pignie, E. Reisner, G. Jeschke, B. V. Lotsch, *Angew. Chem. Int. Ed. Engl.* **2017**, *56*, 510; d) M. Schulz, N. Hagmeyer, F. Wehmeyer, G. Lowe, M. Rosenkranz, B. Seidler, A. Popov, C. Streb, J. G. Vos, B. Dietzek, *J. Am. Chem. Soc.* **2020**, *142*, 15722; e) S. Amthor, S.

Knoll, M. Heiland, L. Zedler, C. Li, D. Nauroozi, W. Tobaschus, A. K. Mengele, M. Anjass, U. S. Schubert, B. Dietzek-Ivansic, S. Rau, C. Streb, *Nat. Chem.* **2022**, *14*, 321.

[6] a) H. Furukawa, K. E. Cordova, M. O'Keeffe, O. M. Yaghi, *Science* **2013**, *341*, 1230444; b) M. C. So, G. P. Wiederrecht, J. E. Mondloch, J. T. Hupp, O. K. Farha, *Chem. Commun.* **2015**, *51*, 3501; c) C.-C. Hou, H.-F. Wang, C. Li, Q. Xu, *Energy Environ. Sci.* **2020**, *13*, 1658; d) X. Liang, X. Zhou, C. Ge, H. Lin, S. Satapathi, Q. Zhu, H. Hu, *Org. Electron.* **2022**, *106*, 106546; e) B. Gibbons, M. Cai, A. J. Morris, *J. Am. Chem. Soc.* **2022**, *144*, 17723; f) C.-A. Tao, Y. Li, J. Wang, *Coord. Chem. Rev.* **2023**, *475*, 214891.

[7] a) Y. Pan, J. Wang, S. Chen, W. Yang, C. Ding, A. Waseem, H. L. Jiang, *Chem. Sci.* **2022**, *13*, 6696; b) P. M. Stanley, F. Sixt, J. Warnan, *Adv. Mater.* **2023**, *35*, 2207280.

[8] a) M. Bourrez, F. Molton, S. Chardon-Noblat, A. Deronzier, *Angew. Chem. Int. Ed. Engl.* **2011**, *50*, 9903; b) M. A. Gonzalez, S. J. Carrington, N. L. Fry, J. L. Martinez, P. K. Mascharak, *Inorg. Chem.* **2012**, *51*, 11930; c) J. Agarwal, C. J. Stanton Iii, T. W. Shaw, J. E. Vandezande, G. F. Majetich, A. B. Bocarsly, H. F. Schaefer Iii, *Dalton Trans.* **2015**, *44*, 2122; d) K. E. Dalle, J. Warnan, J. J. Leung, B. Reuillard, I. S. Karmel, E. Reisner, *Chem. Rev.* **2019**, *119*, 2752.

[9] a) K. A. Grice, C. P. Kubiak, in *Advances in Inorganic Chemistry, Vol. 66* (Ed.: R. v. E. Michele Aresta), **2014**, pp. 163–188; b) A. Sinopoli, N. T. La Porte, J. F. Martinez, M. R. Wasielewski, M. Sohail, *Coord. Chem. Rev.* **2018**, *365*, 60.

[10] C. H. Sharp, B. C. Bukowski, H. Li, E. M. Johnson, S. Ilic, A. J. Morris, D. Gersappe, R. Q. Snurr, J. R. Morris, *Chem. Soc. Rev.* **2021**, *50*, 11530.

[11] A. J. Blake, N. R. Champness, T. L. Easun, D. R. Allan, H. Nowell, M. W. George, J. Jia, X. Z. Sun, *Nat. Chem.* **2010**, *2*, 688.

[12] a) H. Fei, M. D. Sampson, Y. Lee, C. P. Kubiak, S. M. Cohen, *Inorg. Chem.* **2015**, *54*, 6821; b) T. E. Rosser, C. D. Windle, E. Reisner, *Angew. Chem. Int. Ed. Engl.* **2016**, *55*, 7388.

[13] W. C. Henke, C. J. Otolski, W. N. G. Moore, C. G. Elles, J. D. Blakemore, *Inorg. Chem.* **2020**, *59*, 2178.

[14] a) I. Senkovska, F. Hoffmann, M. Fröba, J. Getzschmann, W. Böhlmann, S. Kaskel, *Microporous Mesoporous Mater.* **2009**, *122*, 93; b) E. D. Bloch, D. Britt, C. Lee, C. J. Doonan, F. J. Uribe-Romo, H. Furukawa, J. R. Long, O. M. Yaghi, *J. Am. Chem. Soc.* **2010**, *132*, 14382; c) T. Zhou, Y. Du, A. Borgna, J. Hong, Y. Wang, J. Han, W. Zhang, R. Xu, *Energy Environ. Sci.* **2013**, *6*, 3229; d) X. Deng, J. Albero, L. Xu, H. Garcia, Z. Li, *Inorg. Chem.* **2018**, *57*, 8276; e) L. Chen, Z. Cheng, X. Peng, G. Qiu, L. Wang, *Anal. Methods* **2021**, *14*, 44.

[15] B. A. Johnson, A. M. Beiler, B. D. McCarthy, S. Ott, *J. Am. Chem. Soc.* **2020**, *142*, 11941.

[16] a) F. Carson, S. Agrawal, M. Gustafsson, A. Bartoszewicz, F. Moraga, X. Zou, B. Martin-Matute, *Chem. Eur. J.* **2012**, *18*, 15337; b) D. Sun, Y. Gao, J. Fu, X. Zeng, Z. Chen, Z. Li, *Chem. Commun.* **2015**, *51*, 2645; c) X. Deng, Y. Qin, M. Hao, Z. Li, *Inorg. Chem.* **2019**, *58*, 16574.

[17] a) E. Gore-Randall, M. Irwin, M. S. Denning, J. M. Goicoechea, *Inorg. Chem.* **2009**, *48*, 8304; b) Y. Li, L. Li, Y. Wu, Y. Li, *J. Phys. Chem. C* **2017**, *121*, 8579; c) M. Stanbury, J.-D. Compain, M. Trejo, P. Smith, E. Gouré, S. Chardon-Noblat, *Electrochim. Acta* **2017**, *240*, 288.

[18] K. Kalyanasundaram, J. Kiwi, M. Grätzel, *Helv. Chim. Acta* **2004**, *61*, 2720.

[19] D. A. Kurtz, K. R. Brereton, K. P. Ruoff, H. M. Tang, G. A. N. Felton, A. J. M. Miller, J. L. Dempsey, *Inorg. Chem.* **2018**, *57*, 5389.

[20] a) Gerard J. Stor, Sara L. Morrison, Derk J. Stufkens, A. Oskam, *Organometallics* **1994**, *13*, 2641; b) C. W. Machan, M. D. Sampson, S. A. Chabolla, T. Dang, C. P. Kubiak, *Organometallics* **2014**, *33*, 4550; c) H. Shirley, S. Parkin, J. H. Delcamp, *Inorg. Chem.* **2020**, *59*, 11266; d) M. H. Rønne, M. R. Madsen, T. Skrydstrup, S. U. Pedersen, K. Daasbjerg, *ChemElectroChem* **2021**, *8*, 2108.

[21] H. Koizumi, H. Chiba, A. Sugihara, M. Iwamura, K. Nozaki, O. Ishitani, *Chem. Sci.* **2019**, *10*, 3080.

[22] F. M. Wisser, P. Berruyer, L. Cardenas, Y. Mohr, E. A. Quadrelli, A. Lesage, D. Farrusseng, J. Canivet, *ACS Catal.* **2018**, *8*, 1653.

[23] a) J. J. Walsh, C. L. Smith, G. Neri, G. F. Whitehead, C. M. Robertson, A. J. Cowan, *Faraday Discuss.* **2015**, *183*, 147; b) C. J. Stanton, 3rd, C. W. Machan, J. E. Vandezande, T. Jin, G. F. Majetich, H. F. Schaefer, 3rd, C. P. Kubiak, G. Li, J. Agarwal, *Inorg. Chem.* **2016**, *55*, 3136; c) J. J. Walsh, G. Neri, C. L. Smith, A. J. Cowan, *Organometallics* **2018**, *38*, 1224; d) E. E. DeLuca, T. Chan, J. M. Taylor, B. Lee, R. R. Prabhakar, C. P. Kubiak, *ACS Catal.* **2024**, *14*, 2071.

[24] T. Watanabe, K. Honda, *J. Phys. Chem.* **1982**, *86*, 2617.

[25] a) R. F. Fenske, R. L. DeKock, *Inorg. Chem.* **1970**, *9*, 1053; b) J. E. Vandezande, H. F. Schaefer, *Organometallics* **2018**, *37*, 337.

[26] a) V. Yempally, S. Moncho, F. Hasanayn, W. Y. Fan, E. N. Brothers, A. A. Bengali, *Inorg. Chem.* **2017**, *56*, 11244; b) K. Y. Cohen, R. Evans, S. Dulovic, A. B. Bocarsly, *Acc. Chem. Res.* **2022**, *55*, 944.

[27] a) A. Panagiotopoulos, K. Ladomenou, D. Sun, V. Artero, A. G. Coutsolelos, *Dalton Trans.* **2016**, *45*, 6732; b) P. M. Stanley, A. Y. Su, V. Ramm, P. Fink, C. Kimna, O. Lieleg, M. Elsner, J. A. Lercher, B. Rieger, J. Warnan, R. A. Fischer, *Adv. Mater.* **2023**, *35*, 2207380.

[28] Y.-H. Chiu, T.-F. Chang, C.-Y. Chen, M. Sone, Y.-J. Hsu, *Catalysts* **2019**, *9*, 430.

[29] a) F. Podjaski, J. Kroger, B. V. Lotsch, *Adv. Mater.* **2018**, *30*, 1705477; b) A. Gouder, B. V. Lotsch, *ACS Energy Lett.* **2023**, *8*, 3343.

Manuscript received: April 3, 2024
Version of record online: July 29, 2024